THE EFFECTS OF INFRAGRAVITY ENERGY AND STORM-INDUCED CURRENT ON SHORT WAVES BEYOND THE SURF ZONE

Hans R. Moritz

U.S. Army Corps of Engineers, Portland District
Portland, Oregon USA

1. INTRODUCTION

As storm-induced waves propagate shoreward, from the continental shelf to the shore face, the waves are transformed due to decreasing water depth and the interaction with nearshore circulation. Accurate estimation of storm wave kinematics and related environmental impact is a central theme for many aspects of maritime and coastal margin activity. Proper description of the nearshore wave environment is contingent upon the accurate representation of wave transformation phenomena. This paper highlights two distinct types of storm-related wave phenomena that have been observed in the nearshore waters of the Pacific Northwest coast of the U.S. These phenomena include:

1) **Infra-gravity energy** which can produce a transient water surface (η)
2) The presence of a storm-induced **coastal current** (U_o).

The infra-gravity energy that is associated with groups of large waves can produce η-transients with amplitude of 1 meter and period of 100-400 seconds. Strong surface winds (stress) associated with intense maritime low pressure systems, can produce depth-averaged current (U_o) of 1 meter/sec on the inner shelf. The storm-induced coastal current can be uniform through the water column to depths of 35 m and is typically aligned with the direction of wave propagation along the mid-shelf. The above phenomena may have an underlying but significant effect upon the nearshore wave environment during storms. Investigating the potential effect of these phenomena on nearshore waves provided the motivation for this paper. This paper will refer to wind generated waves (i.e. short-waves, having period = 3-30 seconds) as "waves". Long waves (i.e. waves having period greater than 30 seconds) are considered infra-gravity (IG) waves.

The oceanographic data featured in the paper was acquired offshore the mouth of the Columbia River (MCR), Oregon and Washington, during 1997-1999 and 2003. Current profiles and bottom pressure and current (PUV) data were measured on bottom-deployed tripods in water depth of 13-35 meters. Figure 1 shows relevant data collection sites within context of the bathymetry offshore of MCR. This paper is organized into three parts. Part I describes the general environment at the MCR and the instrumentation/data sampling used to measure parameters of interest. Part II describes the data and functional relationships used to investigate the effect of storm-induced coastal current (U_o) upon nearshore waves. Part III identifies the pulsating nature of infra-gravity energy which can produce a transient water surface (η) during storm conditions and investigates the potential effect upon nearshore waves.

2. PART I: PHYSICAL SETTING AND ENVIRONMENT

In the northeast Pacific Ocean during winter, weather fronts associated with maritime cyclonic storms can extend over the ocean for 1000's of km and cover a latitude difference of 25 degrees. When these maritime low-pressure systems make land fall on the U.S. Pacific Northwest, the coast can be subjected to

hurricane-like conditions. Offshore MCR, wind fields associated with intense winter maritime low-pressure weather systems can create sustained wind speeds greater than 20m/s for fetches greater than 200 km. The resulting wind stress can produce ocean waves greater than 10 m high and a "set-up" of the mean water level of 0.3-1.3 m (storm surge for 1-6 hours duration), depending on storm evolution . The ocean entrance at MCR is characterized by large waves and strong currents and has been considered one of the world's most dangerous coastal inlets. The sea state at the jettied river entrance during storm conditions is characterized by high swell approaching from the northwest to southwest combined with locally generated wind waves from the south to southwest. During October-April average wave height and period is 2.7 m and 12 seconds, respectively. During May-September, average wave height and period is 1.5 m and 9 seconds, respectively. Astronomical tides at MCR are mixed semi-diurnal with a diurnal range of 2.6m. The instantaneous flow rate of estuarine water through the MCR during ebb tide can reach 51,000 m3/sec. Tidally dominated currents within the MCR can exceed 2.5 meter/sec. The transition from coastal regime to oceanic is abrupt. Excluding Astoria Canyon, which is about 17 km offshore, the continental shelf is within 30 km offshore from the MCR. The scale of wind, waves, and currents at MCR is consistently larger than at most coastal locations, providing an opportunity to observe the interaction of coastal processes that may otherwise not be possible.

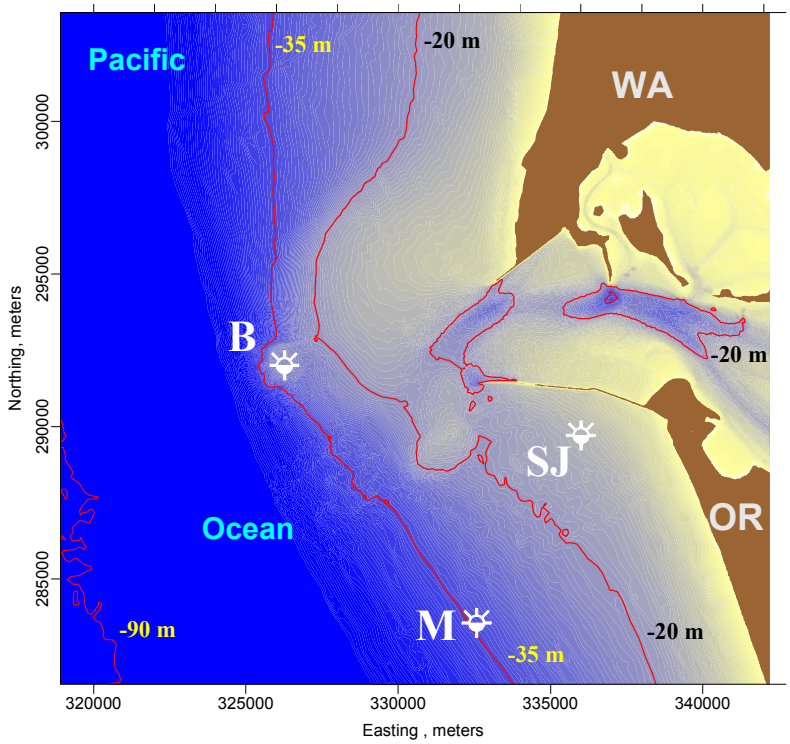

Figure 1. Mouth of the Columbia River, Oregon and Washington USA. Orientation is E-W, N-S. The Distance between north and south jetties is about 3 km. Location of 3 instrumented tripods (via bottom deployment) is shown as Site B, Site M, and Site SJ. Tripods at Sites B and M were deployed 1997-1999. Site SJ tripod was deployed in fall 2003.

2.1 Prototype Data Collection

The focus of this paper involves the analysis of wave and current data acquired at Sites **B** (depth=19 m), **M** (depth=35 m), and **SJ** (depth=14 m), to evaluate the effects of storm related current and IG energy upon nearshore waves. The overall data collection effort described herein was sponsored by the U.S. Army Corps of Engineers (MCNP program) and U.S. Environmental Protection Agency (ODMDS monitoring program) to evaluate the fate of dredged material placed in open water. Site B was located 6 km west (offshore) of MCR on the top of a 25 m tall sand mound created by the disposal of dredged material. The circulation at Site B was influenced both by open ocean (mid shelf) conditions and by tidal

dynamics associated with ebb flow from the MCR. Site M was located 6 km offshore (west) and 5 km south of MCR, away from the first order effects of the MCR estuary. Site SJ is located 1 km south of the MCR south jetty and is outside the direct effect of the estuary, but is subject to circulation caused by the presence of the south jetty.

Relevant instrumentation included: an upward pointed Acoustic-Doppler current Profiler (ADP), downward pointed Acoustic Doppler Velocimeter (ADV), a high precision quartz-digital pressure sensor (Paros-QDPS), and power/data storage units. This instrumentation utilized the SonTek "Hydra," which allowed simultaneous logging of data with a single time stamp. Recorded data relevant to this paper includes bottom pressure (QDPS or P), wave-modified bottom current (ADV or UV), and current thru the water column (ADP). The sampling protocol used for each deployment location is given in table 1. Instrumentation was installed on 2-meter tall tripods that were deployed on the seabed, for periods of 6 weeks to 4 months.

Table 1. Sampling Protocol for Deployments at Sites B, M, and SJ.

Instrument	Parameter	*Sampling Location* Vertical Distance off Seabed	*Sampling* Rate	*Protocol* Duration	Interval
ADV	Bottom Current	57 cm (B and M), 88 cm (SJ)	4 Hz(B),1 Hz(M), 2 Hz(SJ)	1024 sec	180 min
ADP	Current Profile	2 m to water surface	1 Hz	600 sec	180 min
QDPS	Bottom Pressure	83 cm (B and M), 105 cm (SJ)	4 Hz(B),1 Hz(M), 2 Hz(SJ)	1024 sec	180 min .

ADV freq =5 MHz, ADP freq (deployed @ B) = 1500 KHz-1 m bins, ADP freq @ SJ and M = 500 KHz-2 m bins
The vertical distance between sampling point and seabed varied between 57-10 cm during deployment
Sampling duration of ADV and QDPS at site M was 2048 sec

3. PART II: DATA ANALYSIS & FUNCTIONAL RELATIONSHIPS

Part II of the paper discusses the procedure and challenges of using PUV data (as measured near the bed) to describe wind-waves on the water surface (η). Special consideration is given when dealing with an ambient storm-induced current (U_o). Without the aid of a fixed surface-piercing structure, it is not possible to directly observe the detailed behavior of surface gravity waves at offshore locations (i.e. time-varying water surface elevation, $\boldsymbol{\eta(t)}$). Instead, subsurface pressure measurements (usually obtained from a platform on the seabed) can be used to remotely observe surface waves passing overhead. For the data described in this paper, the near-bed pressure (***Pt***, due to the time-varying fluctuation of the water surface) was measured concurrently with bottom current using the sampling protocol in table 1. This produced a PUV data set (Pressure, U- and V- bottom current component) which was used to calculate directional wave spectra for each 1024-second burst. The above method, in part, uses Eq. 1 to estimate the spectra for η (and ultimately calculate a characteristic wave height and period, Hmo and Tp).

Pt*otal = static pressure (averaged over burst) + dynamic pressure (due to waves)* **(1)**

The first term on the right hand side of Eq. 1 is the hydrostatic pressure due to the presence of waves. The second term, is the dynamic pressure associated with the kinematics of progressive waves. In the case of linear wave theory (LWT), time-varying ***dynamic pressure*** (Pd) is related to $\boldsymbol{\eta(t)}$ by employing equations 1-5 along with UV data and other transformations to determine directional wave parameters [Dean & Dalrymple 1984 and Earle et al 1995]. There are two issues that can complicate the use of PUV data to estimate $\boldsymbol{\eta(t)}$ and related statistics: 1) Pressure is attenuated exponentially with increasing depth as described by the pressure response factor [equation 5, below]; and 2) The presence of strong current thru the water column can bias the estimation of wave parameters by Doppler-shifting of observed higher frequency wave components.

$\boldsymbol{Pt}otal = -\rho gz + \rho g\boldsymbol{\eta}\{\cosh[k(d-z)] / \cosh[kd]\}$ *(phase arg), using LWT* **(2)**

$\boldsymbol{Pd}ynamic = \rho g\boldsymbol{\eta}\{\cosh[k(d-z)] / \cosh[kd]\}$ *(phase arg) = Ptotal - Pstatic* **(3)**

$\boldsymbol{\eta}(t) = Pd / [\rho\, g\, \boldsymbol{Kp}(z)]$ *(phase arg), where* **(4)**

$\boldsymbol{Kp}(z) = \cosh[k(d-z)] / \cosh[kd]$ **(5)**

$\boldsymbol{\sigma} = \{\boldsymbol{U_o}k\} + (gk \tanh[kd])^{1/2}$ *= dispersion equation,* $\boldsymbol{U_o}k$ is normally not included **(6)**

d = total depth, η = time-varying displacement of water surface elevation (WSE)
z = depth of measurement, k = 2π/L, σ = 2πf, f = wave frequency = 1/T, L = wave length,
Kp = pressure response factor, T = wave period, Uo = current component affecting waves
Hmo = zero-moment wave height 4(area under energy density spectrum)* $^{1/2}$*, from* $\boldsymbol{\eta}(t)$
Tp = wave period that corresponds with peak energy band of wave spectrum, from $\boldsymbol{\eta}(t)$
NOTE: tide elevation (or total d) and z were known and used to process each burst.

3.1 Functional Relationships

Depth-related pressure attenuation limits the frequency (cut-off) at which waves can be resolved and is a function of the pressure sensor sensitivity (limiting signal/noise ratio), irregardless of instrument sampling rate. The limiting signal/noise ratio for the QDPSs deployed at MCR was found to be 0.033 based upon instrument specifications (verified by plotting the ratio of Pd(f)/Kp(f)). Using equation 5 (substituting 0.033 for Kp) and solving for the frequency (f, or 1/T) corresponding to the wave number (k), the cut-off frequency for Site M was determined to be 0.166 Hz (0.227 Hz for Site B and 0.281 Hz for Site SJ). To avoid any chance of "noise" being introduced into the data analysis, the cut-off frequency was rounded down to 0.16 Hz for Site M (wave period of 6.2 sec). Before proceeding with the derivation of η for wind waves, the PUV data was low-pass filtered for 0.16 Hz (to remove "noise" beyond the cutoff frequency), and high pass-filtered for 0.02 Hz (to remove longwave effects – which were common). The PUV data should *not* be high-pass filtered when analyzing for long wave (IG) effects (see Part III).

To solve for η (WSE), the wave number (k) must be determined from the frequency of the observed waves. If a mean effective current (U_o) is present such that the current is either opposing or following a given wave, then the observed wave period (T) will be Doppler shifted from its intrinsic (without current) value. Based on the data measured at Site M, the *observed* wave period differed from its *intrinsic* value by 0.5 – 4 seconds, depending on current and wave conditions. In this case, the general form of the dispersion equation (Eq. 6, including the terms $\{\boldsymbol{U_o}k\}$) must be used to solve for k from the frequency ($\sigma = 2\pi/T$) of the observed waves. If U_o is present and is not included in the calculation for k, then significant errors may occur in estimating η; resulting in erroneous wave spectra, especially in the higher frequencies and when a strong current is present. If a current was oriented 0° to the wave direction (waves propagating in the direction of current - a *following* condition), there would be no effect on wave direction estimated from PUV data. However, the observed wave period would be smaller than the intrinsic value and the spectral energy density (and Hmo) would be overestimated unless Eq. 6 was used. If the current was oriented 180° to the wave direction (an *opposing* condition), observed wave period would be larger than intrinsic value and spectral energy density would be underestimated. If the angle between waves and currents was 90° (crossing), there would be an effect on wave direction estimated from PUV data, but no appreciable effect on wave period or total spectral density (Hmo); until the waves turn into the current.

3.2 Current Profile at Site B and Effect on PUV Data.

Figure 2 (top 2 panels) summarize the burst-averaged data from approximately 350 bursts acquired at Site B during Aug - Sept 1997. The Columbia River flowrate was relatively constant @ 5,000 m^3/sec. During non-storm periods (periods of little wave action), the magnitude of depth-averaged (ADP) current was heavily modulated by estuary tidal flow, while mean bottom (ADV) current is irregular. During normal conditions, surface current could be much different (speed and direction) than current at mid-depth. During storm events, tidal modulation was diminished, the direction of flow through the water column was uniform, the magnitude of depth-averaged current increased, and the magnitude of the bottom current increased significantly (mean bottom current was driven by flow in the upper water column). During day 25-30, the depth-averaged current at Site B exceeded 1 m/sec. Note that strong currents occurred during periods of large waves. Both were driven by the same process: intense wind stress on the sea surface. During storms, waves and currents progressed in the same direction (following condition).

This paper used the method described by Lee [1990] to estimate the net equivalent current (following or opposing component) affecting waves, and included applying the vector component of depth-scaled current to the wave direction associated with Tp. The estimate for equivalent current is a function of water depth and wave length and is based on the fact that the part of the current closest to the water surface has the greatest influence on waves. The red and black "dots" at the top of the figure 2 indicate "following" (black, uppermost symbols) and "opposing" (red, lower symbols) current-wave conditions, based on the equivalent current. Note that the large storm waves conform to a following current condition.

Overall, the directional alignment of current thru the water column (measured by the ADP) at Site B was highly variable due to the sporadic influence of the Columbia River estuary and open coastal flow. The synopsis of current profile alignment vs. wave direction is: Opposing conditions (current for all ADP bins above the "equivalent current depth" was within 135-225° of wave direction, θw) = 14% of all observations, Following (ADP bins within ± 45° of θw) = 7%, Crossing (ADP bins within 45-135° or 225-315° of θw) = 40% , Others (ADP profile was complex, sheared, not aligned) = 39%. Figure 3 (top panel) illustrates the effect of current on spectral estimates based on PUV data. If a 1 m/s following current is ignored when processing PUV data applicable to Site B, the spectral energy density is overestimated. Note the pronounced effect of current near the higher frequencies of the spectrum. This would be an important consideration for assessing wave transformation, where high frequency energy is transferred to other parts of the spectrum. For the burst shown in the top panel of figure 3, the difference in Hmo between "including" vs. "ignoring" current is about 15% (ie Hmo for ignoring a following current is 15% larger than for correctly including current in spectra calcs). On a deployment-wide basis for Site B, the difference for Hmo between "including" vs. "ignoring" current was 2-20%; depending on current magnitude, direction, and wave properties.

3.3 Effective Current vs. Wave Direction: Comparison of Site B and Site M.

Figure 3B is a pie-chart summary of wave direction vs. effective current alignment for Site B and Site M. Recall the location of site B and Site M (figure1). Site B is heavily influence by tidal circulation of MCR. Site M is beyond the first order effects of tidal flow at MCR and is influenced more by open coast circulation. On a deployment-wide basis for Site M, the difference for Hmo between "including" vs. "ignoring" current was 2-10%; depending on current magnitude, direction, and wave properties.

Based on the pie-charts in figure 3B, Site B has more "opposing" current-wave conditions than Site M (14% of the time vs. 5% of the time). This is because of the ebb tidal flow that affects Site B. Site B also has more "other" current-wave conditions because of the vertically complex nature of tidal flow at Site B (39% vs. 22%). Site M has more "crossing" current-wave conditions (64% vs. 40%), likely because of

the dominance of open coast current (N-S, or along shore) regime at Site M: Waves typically approach from the western quadrant. Currents (opposing or following conditions) affect the incoming waves at Sites B and M during a small percentage of the time. Waves as Site B were affected by "following" or "opposing" currents for 21% of the time; at Site M currents affected waves 14% of the time. This last finding is interesting: The waves at Site M were affected by current during storm conditions, and at Site B during storm conditions or when the tidal circulation was strong enough or aligned correctly to affect incoming waves. It is therefore not a given, that if there is a current present; tben there will be an effect on waves. The exception seems to be during storm conditions, when the current is strong and aligned with the direction of wave propagation.

4. PART III: INFRAGRAVITY ENERGY AND TRANSIENTS IN WAVE CONDITIONS

Figure 4 A-B summarizes the burst-averaged data from 1,020 bursts acquired at Site M during Nov 1998 - Mar 1999. Deployment-averaged wave height (Hmo) was 4 meters and average wave period (Tp) was 12 seconds. The red and black "dots" at the top of the figure 4A indicate "following" (red, uppermost symbols) and "opposing" (black, lower symbols) current-wave conditions, based on the equivalent current. Note that the large storm waves conform to a following current condition. During non-storm periods (Hmo<2m), the (ADP) current thru the water column was irregular and the depth-averaged magnitude was less than 25 cm/s; bottom (ADV) current was weak and irregular. Figure 4B highlights several events when considerable current (0.75 m/sec) was observed throughout the entire water column at Site M, to the seabed depth of 35 m. Note that strong currents occurred during periods of large waves. Both were driven by the same process: intense wind stress on the sea surface. During storm events, the water column exhibited strong sheet flow characteristics: Current was uniform thru depth and depth-averaged current increased to 50-100 cm/s; bottom current magnitude increased to 10-40 cm/s and appeared to be driven by flow in the upper water column.

On 3 March 1999, an intense winter storm offshore the Oregon Coast USA produced southerly windspeeds exceeding 45 m/sec. During the peak of this storm (burst 1013 at 09:00), PUV sensors at Site M indicated a series of waves exceeding 15 meters high (figure 4C). Wave burst data (1Hz for 2048 sec) obtained from the Site M sensors and processed using LWT indicated the following parameters during the peak of the 3 March 1999 storm: Hmo=11.4 m, Tp=16.7 sec, waves approaching from 228 deg (SW). Depth-integrated current was 88 cm/sec flowing toward 320 deg (NW), time-averaged bottom current was 29 cm/sec flowing toward 297 deg (WNW), and instantaneous wave-induced bottom current exceeded 150 cm/sec for both U and V components (figures 4D-E). The effective current and waves were oriented in a "following" condition.

4.1 Infragravity Energy at Site M

To investigate the presence of infra-gravity (IG) energy at Site M during storm wave conditions, the burst data shown in figures 4C-E were processed to remove short-wave and tidal energy. Processing involved the application of a band-pass, 2nd order, zero-phase distortion, elliptic filter, run in forward and reverse directions through the data series. The band-pass range corresponded to 60 seconds to 500 seconds; signals outside this range were truncated according to the filter. To avoid dealing with "end effects" associated with filtering the 2,048 element burst, only the "interior" 1,000 data point of each burst are presented. Results of the infra-gravity filtering for burst M-1013 are shown in figure 5B-D. Figure 5A is the unfiltered signal for η, shown for reference. The IG signal for η (figure 5B) shows infra-gravity (IG) energy displacing the water surface by 0.5 - 1 meter amplitude and having a period of 2-4 minutes. The η IG signal is being modulated by groups of large waves. Total vertical displacement of IG η during the 1,000-second segment was almost 2 meters, which is vertically equivalent to a complete 12-hour tide cycle. It's like tide within a tide, adding another aspect to the reformation of waves as they propagate into

the nearshore. Although the variation of IG η in figure 5B may seem large and unreasonable, the IG variation of bottom current velocity (U and V components, shown in figures 5C-D) is also large (15-20 cm/sec) and tangibly correlated with the η IG signal. Like the η IG signal, the IG pulsating bottom current is also being modulated by groups of large waves. Note how the IG signal for U-velocity component is generally offshore (at 20 cm/sec) while the V-velocity component is generally northward (at 15 cm/sec); or NW vectorally for the entire burst. Waves are approaching from the SW. An explanation for the net offshore and northward movement of bottom water, as indicated in figures 5C-D, is that as the approaching storm waves continually transport momentum/mass to the neashore, a system of return (offshore) flow is established along the bottom. Other wave bursts were processed with similar, but lower magnitude results (not shown here). This effect has been reported in Wright et al (2002) during storm conditions along the Mid-Atlantic and Northern California coasts, but not to the magnitude and duration as observed here. The presence of a sustained offshore flow (of 20 cm/sec) along the bottom of the inner-mid shelf can have profound consequences for sediment transport along the inner shelf and shoreface evolution.

5. CONCLUSIONS

Two distinct types of storm-related wave phenomena have been observed in the nearshore waters (18-35 m depth) of the Pacific Northwest coast of the U.S.: 1) Infra-gravity transients in water level that can approach 1 meter amplitude with 100-400 second period, and 2) Depth-averaged coastal currents of 1 meter/sec which are typically aligned in the direction of wave propagation . If not accounted for, these phenomena have the potential to significantly affect nearshore wind-wave simulation activities (hindcast or forecast).

In this paper it was shown that storm wave energy (height) can be over estimated by 10-20% if the ambient current is not included when processing PUV data collected on the open coast (away from a tidal inlet). In the vicinity of tidal inlets, where circulation can generate effective currents greater than 1 m/sec, omission of the ambient current when processing PUV data can produce over/under-estimates of wave energy by 5-20%, or more. The erroneous effects are greatest near the high frequency part of the spectrum. This can be an important consideration for assessing wave transformation at inlets or during storm conditions. The effect on wave propagation of modulating η by 1-2 meters total displacement within a 17 minute time interval (at Site M), may not be trivial. The presence of IG energy at 35 m water depth motivates the question, "is IG energy at the shore face being driven by surf processes or by processes originating on the mid shelf?, or vice versa?" The effect of such an IG signal on waves propagating in water depth of 20 m or less could lead to surprising results. The nearshore effects of such an IG transient could be significant on modulating short-wave behavior and wave run-up on shore. It is recommended that more work be pursued in defining the conditions under which the phenomena persist and their explicit effect upon wind-wave propagation and characteristics.

6. REFERENCES

Dean, R.G. and Dalrymple, R.A. (1984). " Water Wave Mechanics for Engineers and Scientists", Prentice-Hall, Inc., Englewood Cliffs, NJ, USA.

Earle, M.D., McGehee, D., and Tubman, M. (1995). " Field Wave Gauging Program, Wave Data Analysis Standard," IR-CREC-95-1, USACE, Waterways Experiment Station, Vicksburg, MS

Lee, B.W. (1990). "Wave-Current Interaction: The Equivalent Uniform Current", MS Thesis, University of Liverpool, Liverpool, England.

Wright, L.D., Friedrichs, C.T., and Scully, M.E. (2002). "Pulsation Gravity Driven Sediment Transport on Energetic Shelves", Continental Shelf Research, Vol 22 (2002), pages 2443-2460, Elsevier Science, Ltd.

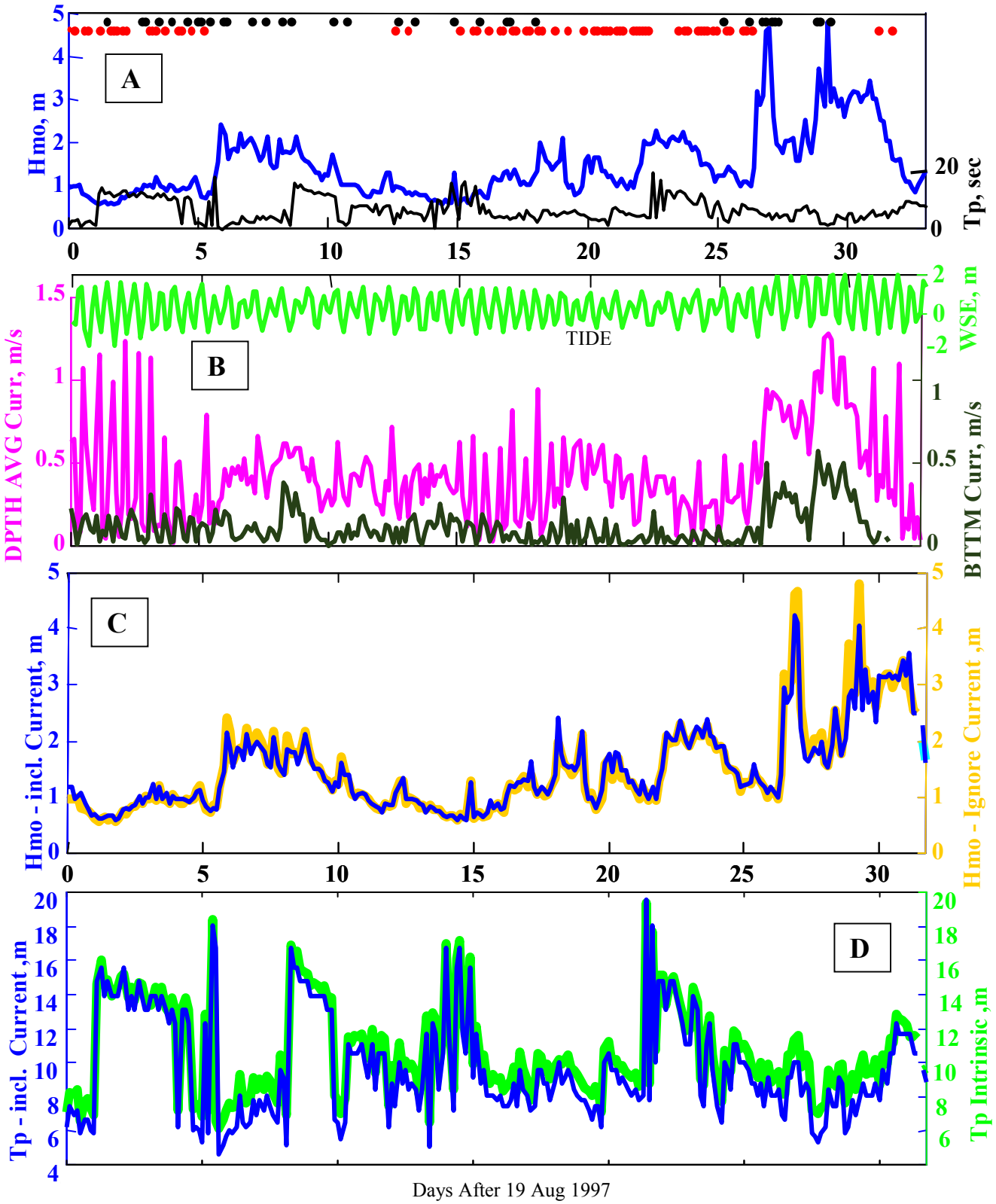

Figure 2. Burst-average statistics for Site B, 0-32 days after 19 Aug 1997. (A) Observed wave height and period. (B) Observed tide, depth averaged current, and bottom current. (C) Comparison of wave height obtained from PUV data including and neglecting mean effective current. (D) Same as C, except for wave period

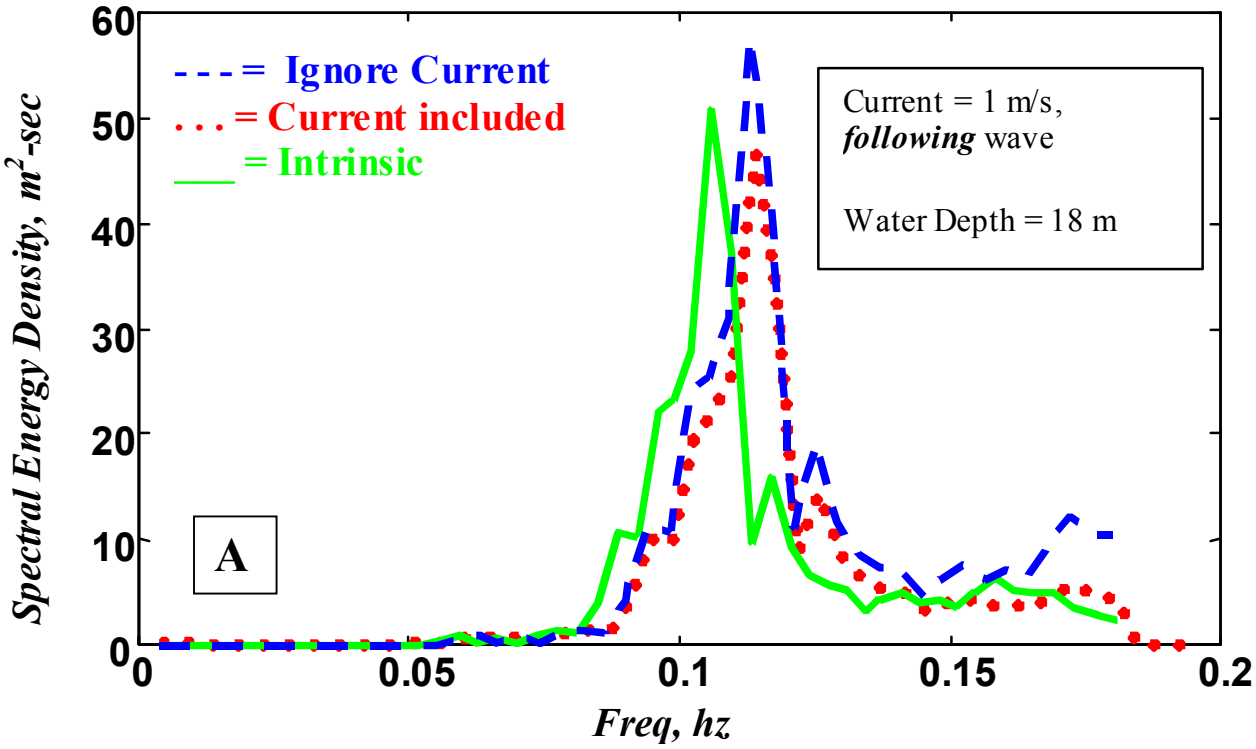

Figure 3A. Seasurface (η) spectral energy density (SED) estimates for a single PUV burst observed on day 28 after 19 Aug 1997 at Site B, illustrating the effect of ambient current on PUV-based spectral density estimates for η. The "Intrinsic" SED is the equivalent spectrum for no current. "Current Included" properly accounts for the presence of current when processing PUV data. Ignoring the ambient current can introduce 15% over-estimate error in wave energy and bias higher end of spectrum.

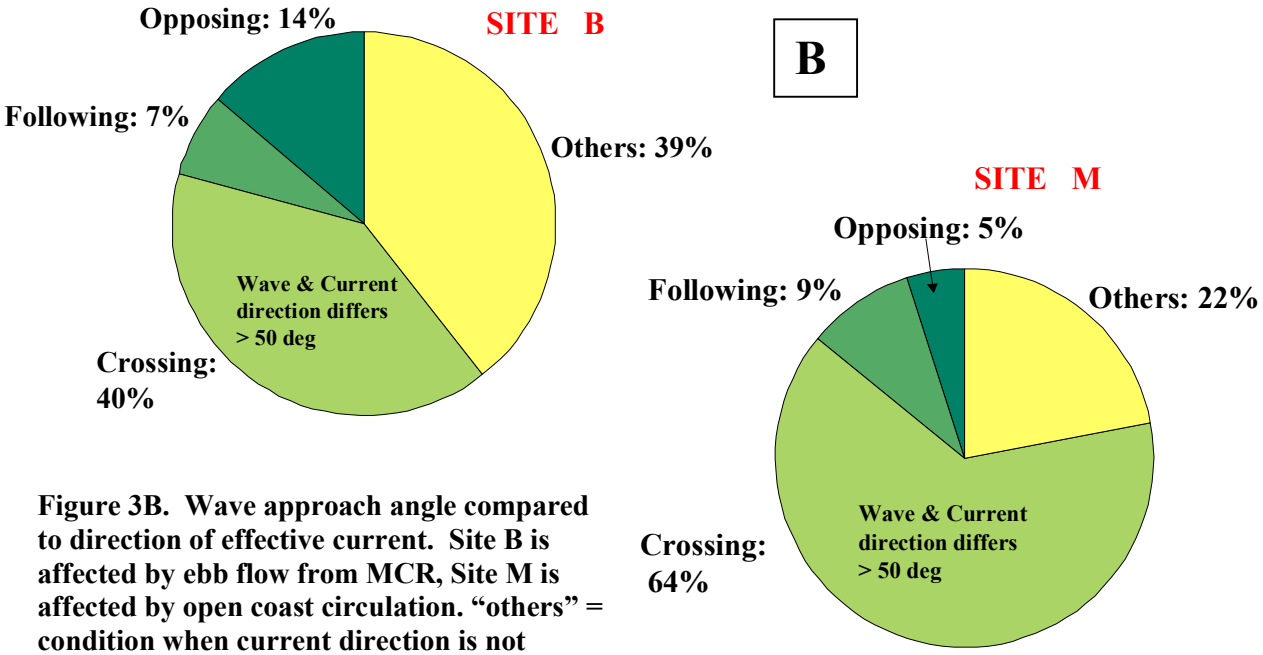

Figure 3B. Wave approach angle compared to direction of effective current. Site B is affected by ebb flow from MCR, Site M is affected by open coast circulation. "others" = condition when current direction is not uniform through the water column

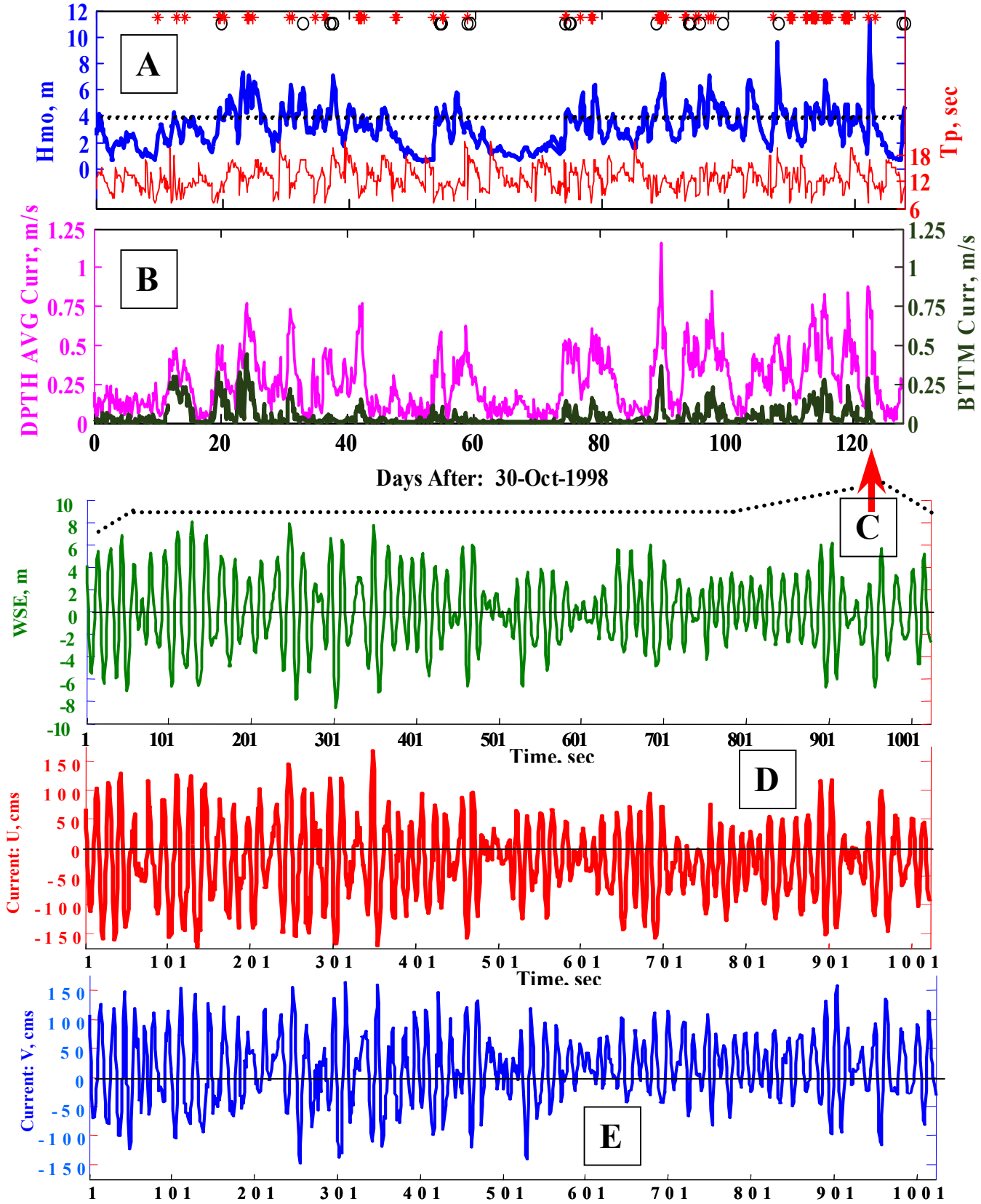

Figure 4. (A-B) Burst averaged data recorded at Site M, 30 Oct 1998–6 Mar 1999. Arrow shows 3 March 1999 09:00 event (burst 1013), featured in C-E of this figure and Part III of this paper.

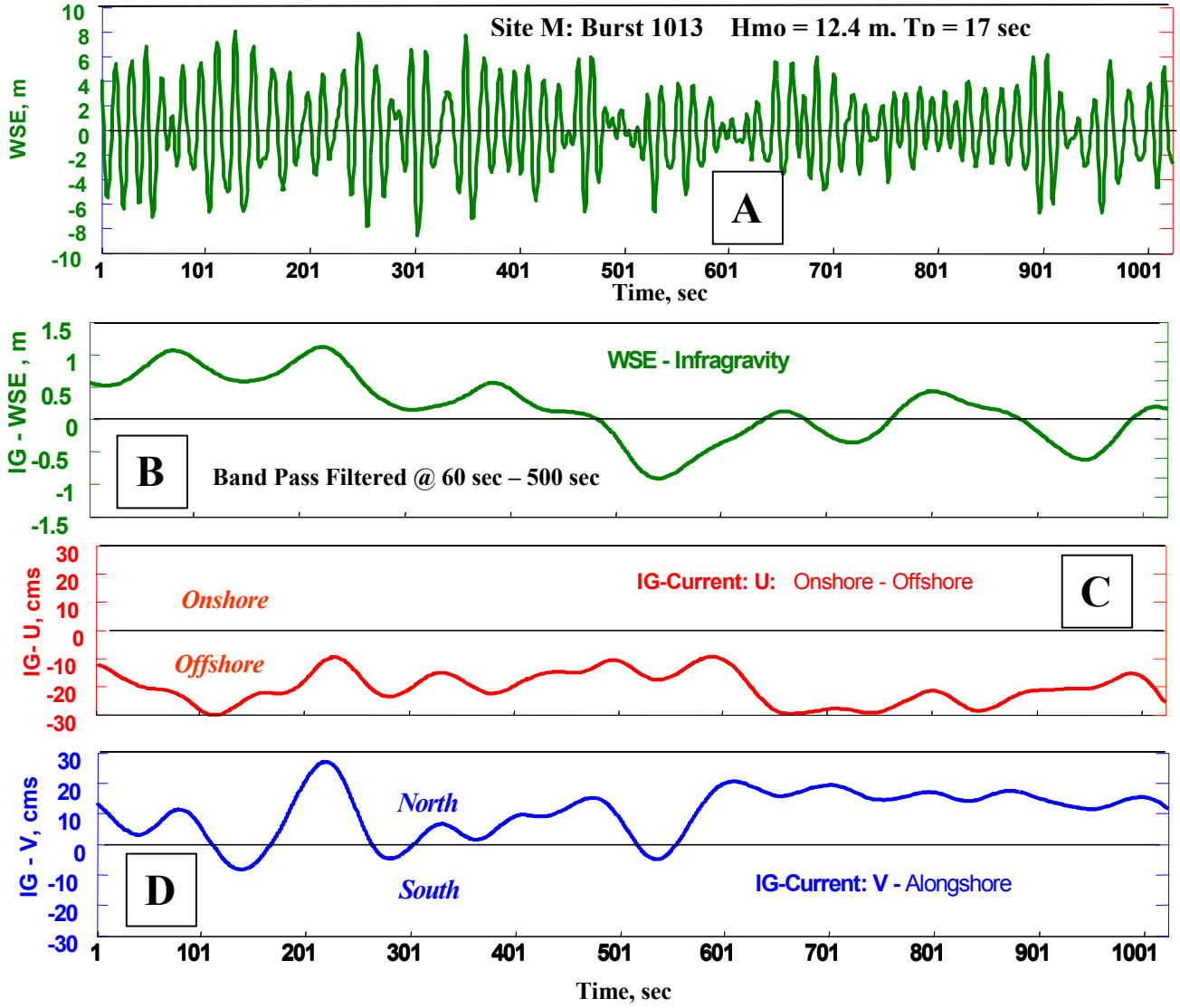

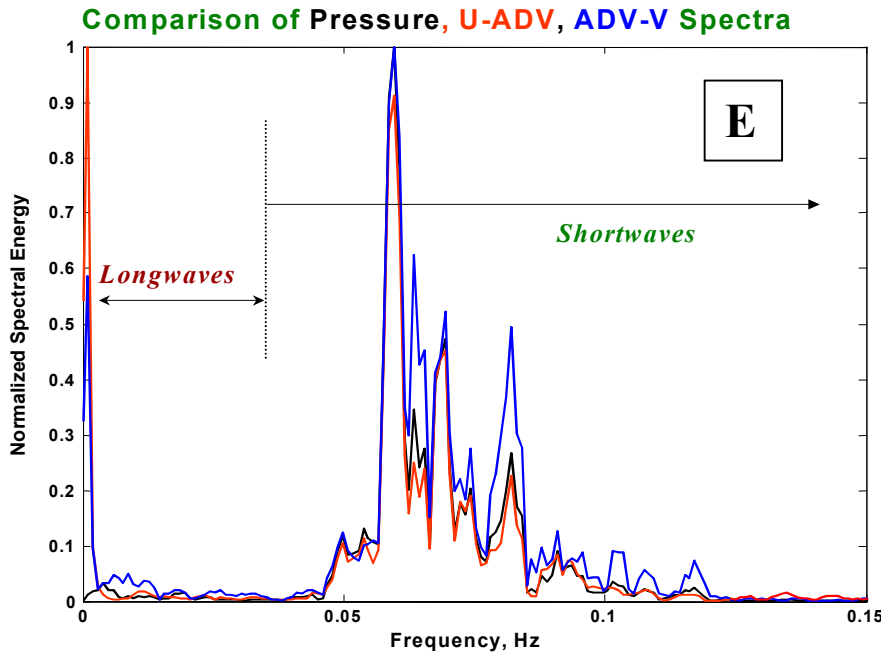

Figure 5. (A) 1000-sec time series from burst 1013 at Site M, during 3 MAR 1999 storm in 35 m depth. (B) Infra-gravity energy within the η record, obtained by bandpass filtering. Note the IG-η amplitude of 1 m. (C-D) Infra-gravity pulsing of bottom current for both U and V components. Note that U is directed offshore (west) and V is directed toward the north. Waves and wind were SSW. (E) Normalized spectral density for PUV data from M-burst 1013. Note presence of IG energy, especially for U and V.